Chemical Geology 306–307 (2012) 114–122

Contents lists available at SciVerse ScienceDirect

Chemical Geology

journal homepage: www.elsevier.com/locate/chemgeo

Strontium sorption and precipitation behaviour during bioreduction in nitrate impacted sediments

Clare L. Thorpe [a], Jonathan R. Lloyd [a], Gareth T.W. Law [a], Ian T. Burke [b], Samuel Shaw [b], Nicholas D. Bryan [a], Katherine Morris [a,*]

[a] Research Centre for Radwaste and Decommissioning and Williamson Research Centre for Molecular Environmental Science, School of Earth, Atmospheric and Environmental Sciences, The University of Manchester, Manchester M13 9PL, UK

[b] Earth Surface Science Institute, School of Earth and Environment, The University of Leeds, Leeds LS2 9JT, UK

ARTICLE INFO

Article history:
Received 20 December 2011
Received in revised form 1 March 2012
Accepted 2 March 2012
Available online 9 March 2012

Editor: J. Fein

Keywords:
Strontium
Bioreduction
Incorporation
Sorption
Nitrate
Nuclear

ABSTRACT

The behaviour of strontium (Sr^{2+}) during microbial reduction in nitrate impacted sediments was investigated in sediment microcosm experiments relevant to nuclear sites. Although Sr^{2+} is not expected to be influenced directly by redox state, bioreduction of nitrate caused reduced Sr^{2+} solubility due to an increase in pH during bioreduction and denitrification. Sr^{2+} removal was greatest in systems with the highest initial nitrate loading and consequently more alkaline conditions at the end of denitrification. After denitrification, a limited re-release of Sr^{2+} back into solution occurred coincident with the onset of metal (Mn(IV) and Fe(III)) reduction which caused minor pH changes in all microcosms with the exception of the bicarbonate buffered system with initial nitrate of 100 mM and final pH > 9. In this system ~95% of Sr^{2+} remained associated with the sediment throughout the progression of bioreduction. Analysis of this pH 9 system using X-ray absorption spectroscopy (XAS) and electron microscopy coupled to thermodynamic modelling showed that Sr^{2+} became partially incorporated within carbonate phases which were formed at higher pH. This is in contrast to all other systems where final pH was <9, here XAS analysis showed that outer sphere Sr^{2+} sorption predominated. These results provide novel insight into the likely environmental fate of the significant radioactive contaminant, ^{90}Sr, during changes in sediment biogeochemistry induced by bioreduction in nitrate impacted nuclear contaminated environments.

1. Introduction

Strontium-90, a high yield fission product resulting from nuclear fuel cycle operations, is a significant radioactive contaminant at nuclear facilities worldwide (Jackson and Inch, 1989; Riley and Zachara, 1992; Mason et al., 2000; Dewiere et al., 2004; McKinley et al., 2007; Priest et al., 2008; McKenzie and Armstrong-Pope, 2010). The behaviour of ^{90}Sr is of particular environmental concern in contaminated land due to both its ~29 year half-life (meaning that it will persist over several hundred years), and it is relative mobility in the shallow sub-surface at some nuclear facilities (McKinley et al., 2007; McKenzie and Armstrong-Pope, 2010). The remediation of ^{90}Sr and other radionuclides (e.g. U and Tc) from groundwaters at these sites is a key challenge for nuclear decommissioning. It is therefore important to explore remediation strategies which show promise of removing or immobilising a wide variety of problematic radionuclides with differing biogeochemical behaviour (e.g. ^{90}Sr, U and Tc) using a single methodology. Furthermore, the geochemical conditions at many nuclear facilities are mildly acidic to neutral, have high nitrate and also have significant naturally occurring iron(III) oxyhydroxide phases that must be taken into account when investigating remediation scenarios (Fredrickson et al., 2004; Istok et al., 2004; Begg et al., 2007; Edwards et al., 2007; McBeth et al., 2007; Law et al., 2010; McKenzie and Armstrong-Pope, 2010).

Strontium-90 exists in the natural environment solely as the Sr^{2+} ion, has very similar geochemical behaviour to Ca^{2+} and is therefore not directly affected by changes in redox conditions. Strontium speciation is controlled primarily by adsorption to mineral surfaces and incorporation or at high concentrations precipitation into Ca^{2+} bearing mineral phases (e.g. $CaCO_3$). Strontium mobility in the subsurface is influenced by the adsorption capacity of the minerals within the sediment as well as the pH and ionic strength of the groundwaters, temperature, organic matter concentration and the exchangeable Ca^{2+}/Mg^{2+} content (Cowan et al., 1991; Chen and Hayes, 1999; Solecki, 2005; Hull and Schafer, 2008; Chiang et al., 2010). The Sr^{2+} ion typically forms outer sphere adsorption complexes which are electrostatically bound to negatively charged mineral surfaces. As expected, increasing adsorption is observed as pH increases above the point of zero charge (PZC) of the relevant mineral phases (Cowan et al., 1991; Ferris et al., 2000; Sahai et al., 2000; Hofmann et al., 2005; Bascetin and Atun, 2006;

* Corresponding author. Tel.: +44 161 275 7541.
E-mail address: katherine.morris@manchester.ac.uk (K. Morris).

0009-2541
doi:10.1016/j.chemgeo.2012.03.001

Bellenger and Staunton, 2008; Chorover et al., 2008). In iron rich sediments, adsorption to both aluminosilicate clays and Fe(III)-oxyhydroxide minerals will have a significant control over Sr^{2+} mobility with pH important in controlling the mineral surface charge and therefore the extent of cation adsorption (Chiang et al., 2010). Clay minerals (eg illite, chlorite, kaolinite and montmorillonite) provide important adsorption surfaces for cations even at low pH due to their relatively low PZC (pH 4–6) and permanent structural charge, (Hussain et al., 1996; Dyer et al., 2000; Coppin et al., 2002; Zhuang and Yu, 2002; Alvarez-Silva et al., 2010) whilst Fe(III)-hydroxides tend to contribute significant adsoption sites at higher pH (PZC pH 7–8) (Small et al., 1999; Hofmann et al., 2005). With increasing pH and alkalinity, groundwater will become oversaturated with regard to carbonate phases and at high Sr^{2+} concentrations, this may allow the precipitation of Sr^{2+} as strontianite ($SrCO_3$) or at lower Sr^{2+} concentrations, the incorporation of Sr^{2+} into $CaCO_3$ phases such as calcite or aragonite (Zachara et al., 1991; Tesoriero and Pankow, 1996; Greegor et al., 1997; Parkman et al., 1998; Finch et al., 2003; Fujita et al., 2004; Mitchell and Ferris, 2005). Additionally, where phosphate is present in the contaminated environment at significant concentrations, the sequestration of Sr^{2+} by phosphate minerals such as apatite is also likely to be a significant control on its behaviour (Handley-Sidhu et al., 2011).

Microbial metabolism has the ability to affect the geochemistry and mineralogy of subsurface sediments, as a result "bioreduction" systems have been considered for the remediation of groundwaters containing the redox active radionuclides Tc and U (Lloyd and Renshaw, 2005). Tc and U have been shown to be immobilised by reduction from the more soluble Tc(VII) and U(VI) to poorly soluble Tc(IV) and U(IV) during Fe(III) reducing conditions (Lloyd, 2003; Law et al., 2010, 2011). As radioactive ^{90}Sr is often found as a co-contaminant in Tc/U contaminated land (Riley and Zachara, 1992; Hartman et al., 2007; McKenzie and Armstrong-Pope, 2010), understanding the behaviour of Sr^{2+} during bioreduction is essential in predicting and managing the mobility of this problematic contaminant in both natural and engineered bioreduction scenarios. During bioreduction the solution pH will be affected by the reaction products which include OH^- and HCO_3^-, and metal reduction will affect sediment mineralogy (Law et al., 2010; Thorpe et al., 2012). Reductive dissolution of bioavailable Fe(III)/Mn oxides and formation of new Fe(II) mineral phases may result in Sr^{2+} that was sorbed to Fe(III) oxide surfaces being released due to mineral dissolution (Langley et al., 2009a, b). However, it has been shown that during Fe(III) oxide crystallisation adsorbed contaminant metals (e.g. Pb^{2+}) can become incorporated into the newly formed phase, therefore, the effect of Fe(III) oxide recrystallisation has the potential to increase or decrease Sr^{2+} environmental mobility. At the same time, the increase in pH caused by bioreduction processes may lead to enhanced removal of Sr^{2+} through increased sorption to mineral surfaces and carbonate precipitation/substitution (Roden et al., 2002; Mitchell and Ferris, 2005; Chorover et al., 2008). Microbial metabolism can result in the production of CO_3^{2-}/HCO_3^- which promotes alkaline pH conditions and supersaturation with regard to carbonate mineral phases ($SrCO_3$ or $CaCO_3$) in which Sr^{2+} can be precipitated (Coleman et al., 1993; Fujita et al., 2004; Mitchell and Ferris, 2005). These processes can also lead to siderite ($Fe(II)CO_3$) formation during microbial reduction of Fe(III), which may result in minor Sr^{2+} becoming incorporated into the newly formed mineral phase (Parmar et al., 2000; Roden et al., 2002).

Here, we consider the effects of microbial metabolism on the biogeochemistry and speciation of Sr^{2+} in conditions relevant to radioactively contaminated sites using stable Sr^{2+} as an analogue for ^{90}Sr. Specifically, sub-surface nitrate concentrations are often elevated and have been reported in excess of 100 mM some nuclear facilities (Riley and Zachara, 1992; Finneran et al., 2002; Fredrickson et al., 2004; Istok et al., 2004; Senko et al., 2005; McKenzie and Armstrong-Pope, 2010). In this study, we have examined the behaviour of Sr^{2+} during the development of bioreducing conditions in sediments representative of the Sellafield nuclear facility that have been amended with between 0.3 and 100 mM nitrate. We tested the hypothesis that an increase in OH^- and CO_3^{2-}/HCO_3^- during nitrate reduction may lead to increased adsorption of Sr^{2+} to mineral surfaces and, once over-saturation was reached, the precipitation and or incorporation of Sr^{2+} into carbonate phases at the high Sr/Ca ratio used in this study (1:1.5). Overall, our aim is to assess whether bioreduction approaches may be relevant to a range of problematic radionuclides including redox active U and Tc as well as ^{90}Sr and thus provide a holistic remediation strategy where co-contamination of these radionuclides occurs.

2. Methods

2.1. Experimental section

2.1.1. Sample collection

Sediments representative of the Quaternary unconsolidated alluvial flood-plain deposits that underlie the UK Sellafield reprocessing site were collected from the Calder Valley, Cumbria, during December 2008 (Law et al., 2010). The sampling area was located ~2 km from the Sellafield site and sediments were extracted from the shallow sub-surface (Lat 54°26′30 N, Long 03°28′09 W). Sediments were transferred directly into sterile containers, sealed, and stored at 4 °C prior to use.

2.1.2. Bioreduction microcosms

Sediment microcosms (10 ± 0.1 g Sellafield sediment, 100 ± 1 ml groundwater) were prepared using a synthetic groundwater representative of the Sellafield region (Wilkins et al., 2007) that was manipulated to produce a range of treatments (Table 1). Aerated systems were first established at variable pH (4.5, 5.5 and 7) to assess Sr^{2+} sorption in oxic systems. Following this a range of sealed microcosm systems were prepared. Unbuffered systems with an initial pH of ~5.5, and representative of the mildly acidic in situ pH at the sample site, were prepared with 0.3, 10, and 25 mM nitrate amendments. Bicarbonate buffered systems with an initial pH of ~7 were prepared with 0.3, 10, 25, and 100 mM nitrate amendments. Sodium acetate was added as an electron donor in excess of available electron acceptors (10 mM for 0.3–10 mM nitrate treatments, 20 mM for 25 mM nitrate treatments and 70 mM for 100 mM nitrate treatments) and a deoxygenated $NaNO_3$ solution was used for NO_3^- amendment. Finally, Sr^{2+} (as stable $SrCl_2$) was added to each microcosm to achieve 1.15 mM (100 ppm). Both the Sr concentration and the solid-solution ratio were chosen to allow full geochemical and spectroscopic characterisation and therefore are very much higher than values of ^{90}Sr encountered at even the most contaminated sites (Riley and Zachara, 1992; McKenzie and Armstrong-Pope, 2010). It should be noted that ^{90}Sr has a relatively

Table 1
Initial geochemical composition of microcosm systems.

System	Initial pH	Nitrate (mM)	Acetate (mM)	Ionic strength
Bicarbonate unamended 0.3 mM nitrate	5.5	0.3	10	0.024
Bicarbonate unamended 10 mM nitrate	5.5	10	10	0.034
Bicarbonate unamended 25 mM nitrate	5.5	25	20	0.059
Bicarbonate amended 0.3 mM nitrate	7	0.3	10	0.027
Bicarbonate amended 10 mM nitrate	7	10	10	0.037
Bicarbonate amended 25 mM nitrate	7	25	20	0.062
Bicarbonate amended 100 mM nitrate	7	100	70	0.190

short half-life and thus high specific activity and even for the most impacted sites where groundwater concentrations of >1000 Bq l^{-1} have been reported the molar concentration of ^{90}Sr will be very low (<10^{-11} mol l^{-1}) compared to our experimental concentrations (Riley and Zachara, 1992; McKinley et al., 2007; Mckenzie and Armstrong-Pope, 2010). Triplicate microcosms were then sealed with buytl rubber stoppers and incubated anaerobically at 20 °C in the dark for 110–250 days. At appropriate time points, sediment slurry was extracted under an O_2 free Ar atmosphere using aseptic technique and centrifuged (15,000 *g*; 10 min) to provide wet sediment pellets and porewater samples for analysis of bioreduction products and strontium.

2.1.3. Geochemical analyses and imaging

During microcosm sampling, total dissolved Fe, Mn(II), and NO_2^- concentrations were measured with standard UV–vis spectroscopy methods on a Jenway 6715 UV–vis spectrophotometer (Goto et al., 1977; Viollier et al., 2000; Harris and Mortimer, 2002). Aqueous NO_3^-, SO_4^{2-}, HCO_3^-/CO_3^{2-} and acetate were measured by ion chromatography (Dionex 4000i liquid chromatography). Aqueous Sr^{2+} and Ca^{2+} were measured by ICP-AES (Perkin-Elmer Optima 5300). Total bioavailable Fe(III) and the proportion of extractable Fe(II) in the sediment was estimated by digestion of ~0.1 g of sediment in 5 ml of 0.5 N HCl for 60 min followed by the ferrozine assay (Stookey, 1970; Lovley and Phillips, 1986). The pH and Eh were measured with a pH/Eh metre (Denver Instruments, UB10) and probes calibrated to pH 4, 7 and 10. Standards were routinely used to check the reliability of all methods and calibration regressions typically had $R^2 \geq 0.99$. The elemental composition and bulk mineralogy of the sediment were determined by X-ray fluorescence (Thermo ARL 9400 XRF) and X-ray diffraction (Philips PW 1050 XRD). Selected end point samples were imaged using Environmental Scanning Electron Microscope (ESEM) in combination with Backscattering Electron Detection (BSE) and Energy Dispersive X-ray Analysis (EDAX) (Philips XL30 ESEM-FG).

2.1.4. X-ray absorption spectroscopy

Selected samples from the bicarbonate buffered pH 7 systems with 10, 25 and 100 mM nitrate amendments were chosen to examine Sr^{2+} speciation in: (1) oxic sterile control pH 7 sediment; (2) Fe(III)/SO_4^{2-} reducing end point pH 7.2 sediments, (3) Fe(III)/SO_4^{2-} reducing end point pH 8.1 sediments; and (4) Fe(III) reducing end point pH 9.3 sediments. Typical concentrations of Sr^{2+} in these samples were in the range 600–1000 ppm. Standards: (1) $SrCl_2$ (aq), 3000 ppm (Fisher Scientific), (2) $SrCO_3$ (s) (Fisher Scientific) and (3) natural Sr^{2+} substituted aragonite from crushed aragonite mineral sample (Sr^{2+} concentration ~1000 ppm), were prepared and diluted with boron nitride where necessary. Samples were transferred to XAS cells under anaerobic conditions, cooled to − 80 K with a liquid nitrogen cryostat (see Nikitenko et al., 2008), and Sr K-edge XAS spectra were collected on beamline BM26A at the European Synchrotron Radiation Facility (ESRF). For sediment samples, Sr K-edge spectra (16115.26 keV) were collected in fluorescence mode using a 9 element solid state Ge detector. Multiple scans were averaged in Athena version 0.8.061 (Ravel and Newville, 2005) and normalised XANES data plotted. Background subtraction for EXAFS analysis was performed using PySpline v1.1 (Tenderholt et al., 2007). EXAFS data were fitted using DLexcurv v1.0 (Tomic et al., 2005) using full curve wave theory (Gurman et al., 1984) by defining a theoretical model which was informed by the relevant literature (e.g. O'Day et al., 2000; Finch et al., 2003) and comparing the model to the experimental data. Shells of backscatterers were added around the Sr^{2+} and by refining an energy correction Ef (the Fermi Energy; which for final fits typically varied between −3.8 and −2.6), the absorber–scatterer distance, and the Debye–Waller factor for each shell. Model iterations were performed until a least squares residual was minimised. Shells were only included in the model fit if the overall least square residual (the R-factor; Binsted et al., 1992) was improved by >5%.

3. Results and discussion

3.1. Sediment characteristics

Sediment composition was measured by X-ray fluorescence and was found to comprise Si (31.57%), Al (7.63%), Fe (3.64%), K (2.79%), Na (0.99%), C (0.96%), Mn (0.87%), Ti (0.45%), Ca (0.23%) and P, S and Cl (<0.1%). We note that XRF analyses show that phosphate is present in our systems at very low concentrations (<0.008%) and is not likely to be a significant control on Sr^{2+} behaviour in this system.

Trace metal analysis showed natural Sr^{2+} to be present in sediments at 62.8 ± 0.2 ppm and natural aqueous Sr^{2+} was <1 ppm. Strontium was added to groundwater media in significant excess to the natural background at 100 ppm (1.15 mM Sr^{2+}) and Ca^{2+} was present at 67 ppm (1.67 mM) thus a Sr/Ca ratio of ~1:1.5 was present in the synthetic groundwater media. The concentration of 0.5 N HCl extractable Fe(III) in the sediment was 5.6 ± 0.5 mmol kg^{-1} prior to incubation and the sediment pH was ~5.5.

3.2. Sorption to oxic sediment

In sterile control microcosms, increased Sr^{2+} sorption was observed in microcosms with a high pH and a low ionic strength. For example, for a constant ionic strength system (I = 0.027 mol dm^{-3}) run at pH 4.5, 5.5 and 7, the Sr^{2+} removal from solution was 35.6 ± 1.9%, 47.4 ± 5.3% and 63.2 ± 2.1% respectively (equating to K_d values of 5.5, 9.0 and 17.1 ml g^{-1}). Differences in strontium behaviour in the sterile microcosms were attributed to pH dependent differences in sorption to mineral surfaces present in the sediment. Sorption to both clays and Fe(III)-oxyhydroxide surfaces is possible although clay minerals is likely to predominate in unbuffered microcosms in which the pH of 4.5–5.5 is above the PZC for many clay minerals (Coppin et al., 2002; Zhuang and Yu, 2002; Alvarez-Silva et al., 2010) whilst Fe-oxyhydroxides become more significant as pH approaches their PZC at pH ~7 (Dyer et al., 2000; Hofmann et al., 2005). Additionally, in control experiments at pH 7 and with increasing ionic strength (0.027, 0.037, 0.062 and 0.190 mol dm^{-3}) resulting from sodium nitrate and sodium acetate additions, Sr^{2+} sorption was 68, 65, 55 and 28% respectively (equating to K_d values of 21.2, 18.5, 12.2 and 3.8 ml/g), presumably reflecting increased competition for Sr^{2+} sorption sites at higher ionic strengths due to cation exchange processes (Hull and Schafer, 2008).

3.3. Biogeochemistry in sediment microcosms

The unbuffered (initial pH 5.5; nitrate range 0.3–25 mM) and bicarbonate buffered (initial pH 7.0; nitrate range 0.3–100 mM) experiments all underwent progressive anoxia and electron acceptors were utilised in the order $NO_3^- > NO_2^- > Mn/Fe(III) > SO_4^{2-}$ (Figs. 1 and 2). Microbially mediated nitrate reduction caused a decrease in porewater nitrate and transient accumulation of nitrite in all systems. The onset of Fe(III) reduction was indicated by an increase in sediment extractable Fe(II) and this was then followed by a decrease in porewater SO_4^{2-} indicating sulfate reduction. No geochemical changes were observed in sterile control microcosms. In unbuffered systems (initial pH 5.5), as expected, microbial activity was inhibited at low pH and terminal electron accepting processes proceeded more slowly than in the parallel bicarbonate buffered microcosms (initial pH 7.0) (Figs. 1 and 2) (e.g. Law et al., 2010; Thorpe et al., 2012). However, in the unbuffered systems, nitrate reduction led to the release of OH^- and HCO_3^-, amending the pH such that a pH increase from 5.5 to 6.8, 7.5 and 8.3 occurred during the reduction of 0.3, 10 and 25 mM nitrate respectively (Fig. 1; Table 2; Thorpe et al., 2012). Metal reduction commenced once nitrate reduction had occurred and mid-point 0.5 N HCl extractable Fe(III) reduction was observed at approximately 25, 35 and 45 days for systems with 0.3, 10 and 25 mM nitrate (Fig. 1). Nitrate reduction and the associated pH increase in all microcosms coincided with removal of Sr^{2+}

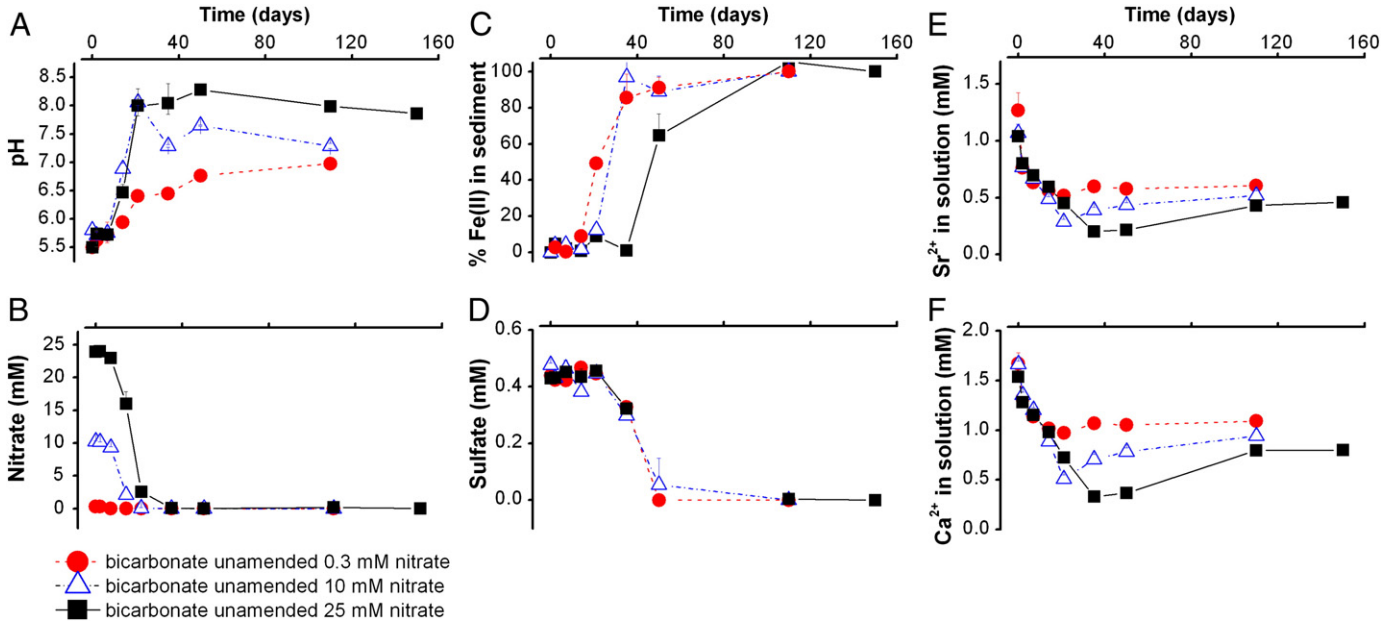

Fig. 1. Unbuffered, microcosm incubation time-series data (days 0−160). (A) pH (B) NO_3^-, (C) 0.5 N HCl % extractable sedimentary Fe as Fe(II), (D) SO_4^{2-}, (E) porewater Sr and (F) porewater Ca. ● = 0.3 mM nitrate system; Δ = 10 mM nitrate system; ■ = 25 mM nitrate system. Initial pH in all microcosms was ~5.5. Error bars represent 1σ experimental uncertainty from triplicate microcosm experiments (where not visible error bars are within symbol size).

and Ca^{2+} from solution (Fig. 1). Interestingly, as bioreduction progressed through Fe(III) and SO_4^{2-} reduction in these dynamic systems, a small amount of both Sr^{2+} and Ca^{2+} (<10% of that sorbed after nitrate reduction) was remobilised to solution. This re-release coincided with a slight decrease in pH (<0.5 pH units) presumably due to re-equilibration of the microcosm system following nitrate reduction. The re-release of sorbed Sr^{2+} and Ca^{2+} may be due solely to pH dependent sorption/desorption to mineral surfaces or in some systems (for example above pH 7) there may be release of Sr^{2+} and Ca^{2+} sorbed to Fe(III)-oxyhydroxides as reductive dissolution of the Fe(III) phases occurred (Small et al., 1999; Roden et al., 2002; Langley et al., 2009a, b).

In bicarbonate buffered systems with an initial pH of 7, the final pH following the reduction of 0.3, 10, 25 and 100 mM nitrate was 7.5, 8.0, 8.5 and 9.4 (Fig. 2: Table 2). Terminal electron accepting processes proceeded faster than in unbuffered microcosms with mid-point 0.5 N HCl extractable Fe(III) reduction occurring at <20 days for 0.3 and 10 mM nitrate systems and around 40 and 160 days for systems with 25 and 100 mM nitrate (Fig. 2). As with the unbuffered systems, Sr^{2+} and Ca^{2+} were removed from solution during nitrate reduction with increasing pH and a small amount (<10% of that sorbed after nitrate reduction) of Sr^{2+} and Ca^{2+} was re-released into solution in all systems apart from the bicarbonate buffered,

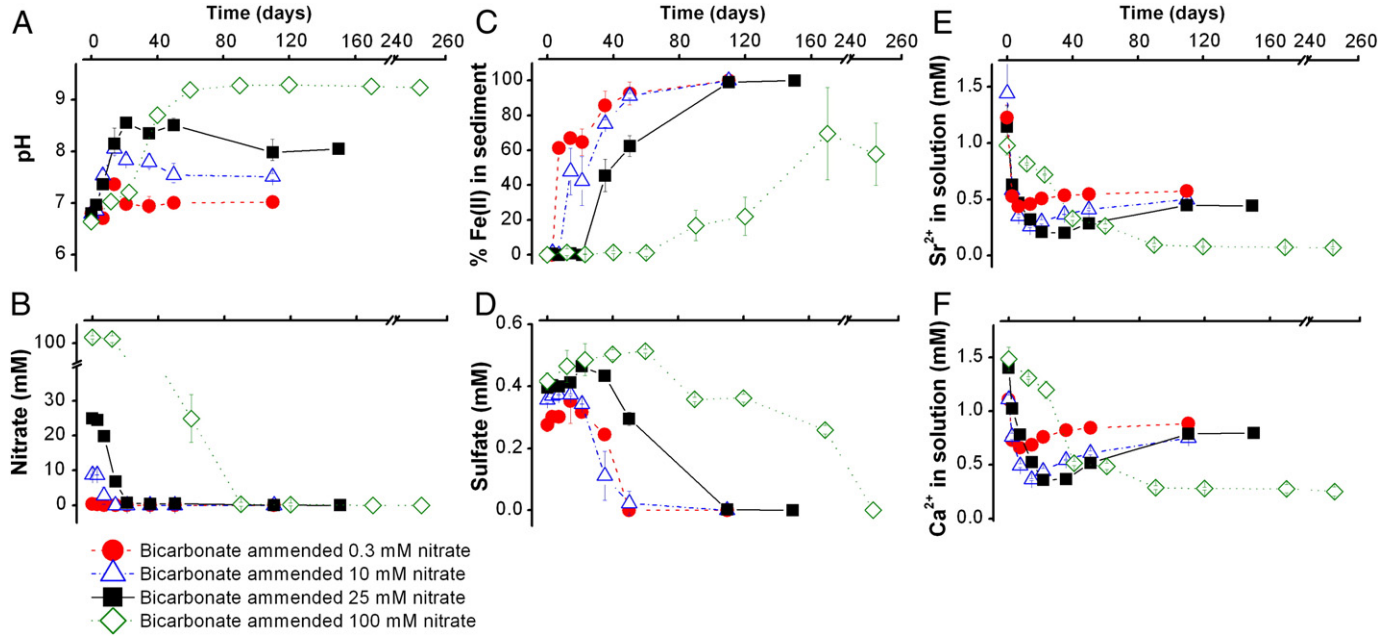

Fig. 2. Buffered, microcosm incubation time-series data (days 0–160/260). (A) pH, (B) NO_3^-, (C) 0.5 N HCl % extractable sedimentary Fe as Fe(II), (D) SO_4^{2-}, (E) porewater Sr and (F) porewater Ca. ● = bicarbonate buffered 0.3 mM nitrate system; Δ = bicarbonate buffered 10 mM nitrate system; ■ = bicarbonate buffered 25 mM nitrate system; ◊ = bicarbonate buffered100 mM nitrate system. Initial pH in all microcosms was ~7. Error bars represent 1σ experimental uncertainty from triplicate microcosm experiments (where not visible error bars are within symbol size).

Table 2
Percentage strontium sorbed to sediments during nitrate and metal reduction compared to an oxic control.

System	Sterile oxic		90% nitrate reduction		90% Fe(III)/SO_4 reduction		End point
	% Sr^{2+} on sediment[a]	pH	% Sr^{2+} on sediment	pH	% Sr on sediment	pH	Net decrease (−) or increase (+) of Sr^{2+} on sediments
Bicarbonate unamended 0.3 mM nitrate	47.0	5.5	54 ± 2.2	6.6	50 ± 2.3	6.7	+~2%
Bicarbonate unamended 10 mM nitrate	47.3	5.5	75 ± 1.8	8.0	55 ± 3.6	7.5	+~9%
Bicarbonate unamended 25 mM nitrate	45.5	5.5	82 ± 2.1	8.2	60 ± 0.5	7.8	+~18%
Bicarbonate amended 0.3 mM nitrate	67.9	7.0	63 ± 1.4	7.0	50 ± 1.8	7.0	−~16%
Bicarbonate amended 10 mM nitrate	64.2	7.0	78 ± 0.7	8.0	57 ± 0.3	7.5	−~6%
Bicarbonate unamended 25 mM nitrate	54.8	7.0	84 ± 0.4	8.5	62 ± 0.7	8.1	+~7%
Bicarbonate unamended 100 mM nitrate	32.6	7.0	93 ± 1.4	9.3	94 ± 0.8	9.3	+~61%

[a] Differences in Sr^{2+} sorption to sterile controls occur due to varying pH and ionic strength due to the addition of $NaHCO_3$, Na-acetate and $NaNO_3$.

100 mM nitrate system (Fig. 2). Here, the final pH was 9.3 and interestingly, Sr^{2+} remained associated with the sediment throughout Fe(III) and sulfate reduction. In this high nitrate loaded system, the utilisation of 70 mM acetate resulted in the accumulation of 207 ± 4.9 mM of dissolved inorganic carbon and amended the pH to alkaline conditions.

For comparison with other studies it is useful to examine distribution coefficients for Sr^{2+} (K_d = (solid in g g^{-1}/aqueous in g ml^{-1})). Distribution coefficients are only relevant to the specific geochemical conditions of each system of study and give an indication of the extent of Sr^{2+} partitioning onto the solid phase in different systems. Here K_d values ranged from <10 ml g^{-1} in systems with a high ionic strength (0.190 mol dm^{-3}) or a low pH (5.5) and increased to >50 ml g^{-1} with increasing pH. The distribution coefficient in systems with a final pH>9 was calculated to be 133 ml g^{-1}. These K_d values compare well with literature values where surface sediment K_d values are typically between 10 and 200 ml g^{-1} (Deldebbio, 1991; Liszewski et al., 1998; Fernandez et al., 2006) and deeper more quartz rich sediments have K_d values of <10 ml g^{-1} (Stephens et al., 1998; Dewiere et al., 2004).

Modelling of the solution chemistry in bioreduced systems (PHREEQC-2: LLNL database) suggested that for all unbuffered bioreduced system end-points, Fe(II)CO_3 and $SrCO_3$ were oversaturated in all the different nitrate amendments whilst the $CaCO_3$ phases were undersaturated in the bioreduced 0.3 mM nitrate amended systems and oversaturated in all other treatments (Table 3). As expected for these carbonate phases, the degree of oversaturation increased as alkalinity increased. In the bicarbonate amended bioreduced system end points, all nitrate amendments showed oversaturation of Fe(II)CO_3, $CaCO_3$, and $SrCO_3$ and with increasing oversaturation with increasing alkalinity (Table 3). Clearly, although unable to resolve the detail of the dynamic bioreduction experiments, these modelling data suggest an increased tendency to oversaturation of carbonate mineral phases with increased nitrate reduction and microbially produced alkalinity.

ESEM (Environmental Scanning Electron Microcoscopy) was used to assess the distribution of Sr^{2+} in end point pH 7 (bicarbonate buffered 10 mM nitrate) and pH 9.3 (bicarbonate buffered 100 mM nitrate) sediments (Fig. 3). In backscattering mode image brightness is related to the average atomic mass present (Z contrast). In the pH 9.3 system, secondary electron and backscatter images in combination with EDAX analysis show a number localised bright spots of ~20 μm diameter enriched in Sr^{2+} (Fig. 3) whilst there were no observed localised bright spots in the pH 7 system. Semi-quantitive analysis of EDAX spectra of the localised bright spots showed a significant concentration of Ca^{2+} and Sr^{2+} in agreement with predicted $SrCO_3$ and $CaCO_3$ oversaturation.

In order to further understand Sr^{2+} speciation during bioreduction in these complex systems, samples from an oxic pH 7 control with Sr^{2+} sorption, and selected bicarbonate buffered, nitrate amended (0.3, 25 and 100 mM) bioreduced end points with a final pH of 7.2, 8.1 and 9.3 were analysed using X-ray absorption spectroscopy. XANES spectra for all samples show a single peak indicative of 9 fold coordination and there was no evidence for 6 fold coordination (as in the calcite standard which has a clear doublet). Thus our experiments show no evidence for Sr^{2+} substituted calcite formation (Fig. 4; Parkman et al., 1998). XANES spectra for the oxic, bioreduced pH 7.2, and bioreduced pH 8.1 samples all comprised a single peak and compared well with a $SrCl_2$ aqueous standard, implying that in these sediments, after bioreduction, Sr^{2+} was present primarily as adsorbed Sr^{2+} (Fig. 4). By contrast, the XANES spectra for the pH 9.3 bioreduced sample showed some evidence for peak flattening and thus some similarity to the model Sr-carbonate phases (e.g. strontianite and Sr-substituted aragonite) (Fig. 4). Modelling of the EXAFS spectra for the oxic, bioreduced pH 7.2 and bioreduced pH 8.1 samples showed an approximate 9-fold coordination environment at 2.60 Å, indicative of outer sphere Sr^{2+} adsorption to mineral surfaces (Parkman et al., 1998; Chen and Hayes, 1999; Carroll et al., 2008; Fig. 5; Table 4). EXAFS for the pH 9.3 bioreduced sample could also be modelled with 9 fold "outer sphere" co-ordination. However, EXAFS model fits for this system were significantly improved by addition of shells of carbon and strontium backscatters at 3.03, 4.18 and 4.87 Å (Table 4; Fig. 5) respectively. This clearly indicates a contribution from an additional Sr^{2+} species in this spectrum with bond distances indicative of $SrCO_3$ (Parkman et al., 1998;

Table 3
Saturation index for key carbonate minerals in microcosm systems. Modelled using PHREEQC-2 (Lawrence Livermore National Laboratory database— llnl.dat).

	Saturation index (PHREEQC-2)[a]					
	Sr^{2+} (ppm)	Final pH	Siderite	Calcite	Aragonite	Strontianite
Oxic sediment	100	5.5	−1.16	−3.52	−3.67	−2.87
Bioreduced sediments	100					
Unbuffered 0.3 mM nitrate	100	6.7	1.97	−0.17	−0.32	0.47
Unbuffered 10 mM nitrate	100	7.5	2.76	0.70	0.55	1.35
Unbuffered 25 mM nitrate	100	7.8	3.07	1.18	1.03	1.83
Bicarbonate buffered 0.3 mM nitrate	100	7.0	2.31	0.22	0.08	0.86
Bicarbonate buffered 10 mM nitrate	100	7.2	2.49	0.42	0.28	1.07
Bicarbonate buffered 25 mM nitrate	100	8.1	3.28	1.48	1.33	2.14
Bicarbonate buffered 100 mM nitrate	100	9.3	3.25	2.36	2.21	3.65
Bicarbonate buffered 100 mM nitrate	10	9.3	3.25	2.36	2.21	2.25
Bicarbonate buffered 100 mM nitrate	1	9.3	3.25	2.36	2.21	1.15
Bicarbonate buffered 100 mM nitrate	0.1	9.3	3.25	2.36	2.21	0.25
Bicarbonate buffered 100 mM nitrate	0.01	9.3	3.25	2.36	2.21	-0.75

[a] Temperature 21 °C, concentration of ions in solution from Table 1, pH as measured.

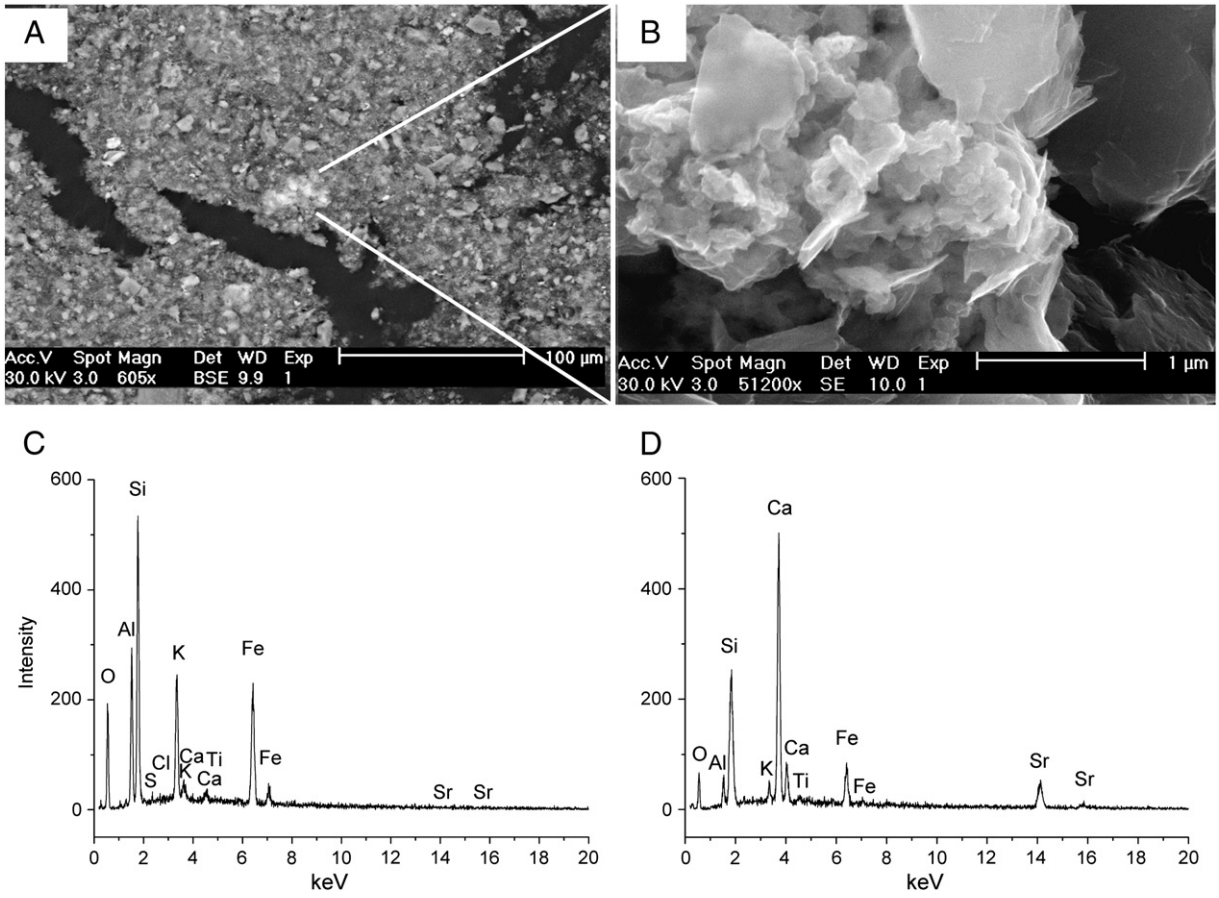

Fig. 3. ESEM images of the Fe(III) reducing bicarbonate buffered 100 mM nitrate sample at final pH 9 containing Sr- and Ca-rich crystalline structures and corresponding EDAX spectra. Images show: (A) ESEM backscatted detection mode image of sediment indicating heavier elements (Sr) as bright patches in the field of view 300 µm; (B) Secondary electron image showing the structure of Sr/Ca rich area at a field of view 3 µm; (C) the energy dispersive electron analysis (EDAX) spectra for the entire sample; and (D) a spot EDAX analysis on the Sr/Ca rich structure.

O'Day et al., 2000). Further analysis showed that a model EXAFS fit was possible with additional shells of 2.6 carbon atoms at 3.03 Å, 2.8 strontium atoms at 4.18 Å and 2.5 strontium atoms at 4.87 Å; these values are approximately 50% of what is expected for pure $SrCO_3$, which is consistent with a model where approximately half of Sr^{2+} is present in a $SrCO_3$ like environment (Table 4; Fig. 5). Indeed, this model, which is geochemically sensible, resulted in a better fit to the spectrum and a 27% reduction in the least square residual when compared to the data modelled as 100% adsorbed Sr^{2+} suggesting that both adsorption and incorporation occurred in this system (Table 4).

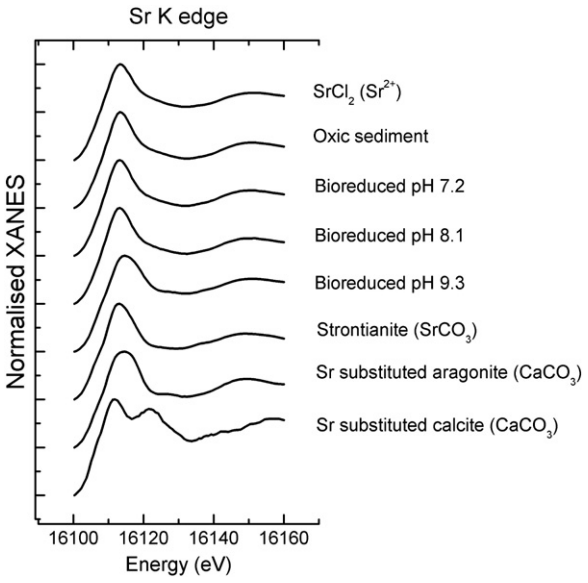

Fig. 4. Normalised Sr K-edge XANES spectra for selected standards and microcosm systems. From top to bottom: $SrCl_2$ aqueous standard, oxic sediment sample, bioreduced pH 7.2 sample, bioreduced pH 8.1 sample, bioreduced pH 9.3 sample, Sr substituted aragonite standard and strontianite standard.

In natural and engineered environments concentrations of Sr^{2+} and ^{90}Sr are generally much lower than in these experiments (eg 0.1 ppm natural Sellafield groundwater) (Wilson, 1996). Under Sellafield conditions, model simulations predicted that bioreduced system even at pH 9 would be undersaturated with regard to $SrCO_3$ below ~0.1 ppm strontium (Table 3); nonetheless, at a pH > 7, systems would remain supersaturated with respect to $CaCO_3$. It is therefore feasible that substitution of Sr^{2+} into $CaCO_3$ rather than precipitation as $SrCO_3$ will be important in controlling the mobility of both natural Sr^{2+} and artificial ^{90}Sr in such systems. Indeed, it is well documented that Sr^{2+} can substitute for Ca^{2+} within the calcium carbonate lattice (Pingitore et al., 1992; Tesoriero and Pankow, 1996; Greegor et al., 1997; Warren et al., 2001; Finch et al., 2003). Recent studies, focused on bacterial urolysis, have found that Sr^{2+} incorporation into the $CaCO_3$ lattice was enhanced by the rapid precipitation rates resulting from HCO_3^- production and the pH rise associated with microbial respiration (Fujita et al., 2004; Mitchell and Ferris, 2005). Both a pH rise and dissolved organic carbon production were observed during bioreduction by indigenous microorganisms in this study suggesting that nitrate reduction might also result in enhanced Sr^{2+} uptake into calcite compared to those observed under slower precipitation rates.

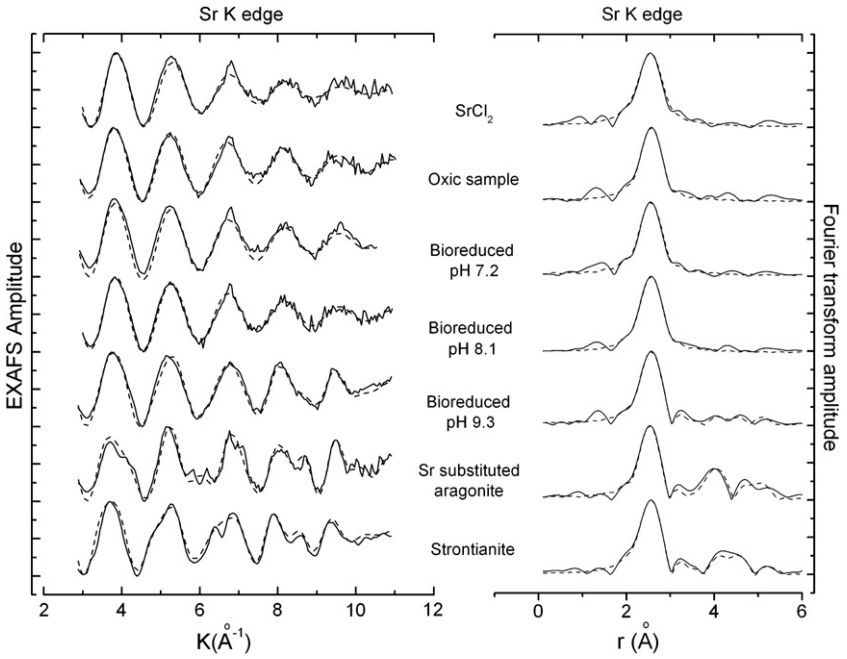

Fig. 5. Experimental (solid) and theoretical best fit (dashed) EXAFS spectra and corresponding Fourier transforms obtained for (from top to bottom): $SrCl_2$ aqueous standard, oxic sediment sample, bioreduced pH 7.2 sample, bioreduced pH 8.1 sample, bioreduced pH 9.3 sample, Sr substituted aragonite standard and strontianite standard. Solid lines are the data and dashed lines are the fits to the data.

3.4. Summary and environmental relevance

Overall, our experiments showed that there is increased Sr^{2+} removal from solution during bioreduction in nitrate impacted sediments compared to sterile control systems. In systems with an initially low pH (5.5), removal of Sr^{2+} from solution after bioreduction was particularly enhanced, presumably due to the increased sorption onto deprotonated mineral surfaces as the pH increased above 6. After nitrate reduction, system re-equilibration and an associated decrease (<0.5 pH units) in pH resulted in modest (<10%) re-release of Sr^{2+} into solution highlighting the vulnerability of adsorbed Sr^{2+} to re-release due to changing geochemical conditions.

Table 4
Parameters obtained from EXAFS data fitting of Sr K-edge spectra from Sr^{2+} associated with sediment at various sediment conditions.

Sample	Shell no	Bond	C.N.	R(Å)	$2\sigma^2$ (Å^2)	R-factor
$SrCl_2$	1	Sr–O	8.75	2.60	0.029	23.0
Oxic sample pH 7	1	Sr–O	8.83	2.61	0.019	22.1
Bioreduced pH 7.2	1	Sr–O	8.68	2.60	0.020	18.0
Bioreduced pH 8.1	1	Sr–O	8.89	2.61	0.021	19.6
Bioreduced pH 9.3 (1)	1	Sr–O	8.03	2.60	0.024	27.9
Bioreduced pH 9.3 (2)	1	Sr–O	8.19	2.61	0.021	20.2
	2	Sr–C	2.68	3.03	0.015	
	3	Sr–Sr	2.78	4.18	0.029	
	4	Sr–Sr	2.47	4.88	0.024	
Strontianite	1	Sr–O	9[a]	2.64	0.027	20.3
	2	Sr–C	6[a]	3.04	0.032	
	3	Sr–Sr	6[a]	4.22	0.029	
	4	Sr–Sr	4[a]	4.97	0.033	
Sr substituted aragonite	1	Sr–O	9[a]	2.59	0.015	29.1
	2	Sr–C	6[a]	2.98	0.031	
	3	Sr–Ca	6[a]	4.02	0.020	
	4	Sr–Ca	4[a]	4.87	0.013	

N is the occupancy (±~25%), R(Å) (is the interatomic distance (±~0.02 Å), $2\sigma^2$ is the Debye–Waller factor (Å^2) and *R* (least squares residual) is a measure of the overall goodness of fit.
[a] Fixed.

In extreme environments with very high (100 mM) nitrate concentrations, bioreduction led to a final pH of >9 and enhanced removal of Sr^{2+} from solution occurred throughout the bioreduction cascade. This study has shown that in very high nitrate systems an increase in pH and dissolved inorganic carbon associated with microbial reduction and particularly denitrification can promote the precipitation and incorporation of Sr^{2+} into carbonate phases although the engineering aspects of this process are as yet unexplored. Clearly, radio-strontium incorporation into carbonate phases is desirable in remediation scenarios as they are redox insensitive phases and are potentially more resistant to remobilization than sorbed Sr^{2+}. It is also clear that bioreduction scenarios have the potential to impact Sr^{2+} mobility in the subsurface and that understanding the bioreduction behaviour of redox inactive radioactive contaminants can be of significance in assessing the efficacy of bioreduction schemes at nuclear facilities. We further suggest that under constrained conditions, bioreduction may have the potential to co-treat redox active radionuclides and ^{90}Sr increasing the range of applications for this clean-up technology across the global nuclear waste legacy.

Acknowledgments

We thank Jon Fellowes, Alastair Bewsher and Paul Lythgoe for help in data acquisition. We also thank the ESRF beamline (B-26) scientists and Sarah Wallace (University of Leeds) for their help in XAS analysis. This work was supported by a studentship to CLT from the Engineering and Physical Science Research Council (EPSRC) as part of the Decommissioning, Immobilisation and Management of Nuclear Waste for Disposal (DIAMOND) consortium: grant EP/F055412/1. We also acknowledge the support of the Natural Environment Research Council grant NE/H007768/1.

References

Alvarez-Silva, M., Uribe-Salas, A., Mirnezami, M., Finch, J.A., 2010. The point of zero charge of phyllosilicate minerals using the Mular–Roberts titration technique. Mining and Engineering 23, 383–389.

Bascetin, E., Atun, G., 2006. Adsorption behavior of strontium on binary mineral mixtures of montmorillonite and kaolinite. Applied Radiation and Isotopes 64, 957–964.
Begg, J.D.C., Burke, I.T., Morris, K., 2007. The behaviour of technetium during microbial reduction in amended soils from Dounreay, UK. Science of the Total Environment 373, 297–304.
Bellenger, J.P., Staunton, S., 2008. Adsorption and desorption of Sr-85 and Cs-137 on reference minerals, with and without inorganic and organic surface coatings. Journal of Environmental Radioactivity 99, 831–840.
Binsted, N., Strange, R.W., Hasnain, S.S., 1992. Constrained and restrained refinement in EXAFS data analysis with curved wave theory. Biochemistry 31, 12117–12125.
Carroll, S.A., Roberts, S.K., Criscenti, L.J., O'Day, P.A., 2008. Surface complexation model for strontium sorption to amorphous silica and goethite. Geochemical Transactions 9, 2.
Chen, C.C., Hayes, K.F., 1999. X-ray absorption spectroscopy investigation of aqueous Co(II) and Sr(II) sorption at clay–water interfaces. Geochimica et Cosmochimica Acta 63, 3205–3215.
Chiang, P.N., Wang, M.K., Huang, P.M., Wang, J.J., Chiu, C.Y., 2010. Cesium and strontium sorption by selected tropical and subtropical soils around nuclear facilities. Journal of Environmental Radioactivity 101, 472–481.
Chorover, J., Choi, S., Rotenberg, P., Serne, R.J., Rivera, N., Strepka, C., Thompson, A., Mueller, K.T., O'Day, P.A., 2008. Silicon control of strontium and cesium partitioning in hydroxide-weathered sediments. Geochimica et Cosmochimica Acta 72, 2024–2047.
Coleman, M.L., Hedrick, D.B., Lovley, D.R., White, D.C., Pye, K., 1993. Reduction of Fe(III) in sediments by sulfate-reducing bacteria. Nature 361, 436–438.
Coppin, F., Berger, G., Bauer, A., Castet, S., Loubet, M., 2002. Sorption of lanthanides on smectite and kaolinite. Chemical Geology 182, 57–68.
Cowan, C.E., Zachara, J.M., Resch, C.T., 1991. Cadmium adsorption on iron-oxides in the presence of alkaline-earth elements. Environmental Science and Technology 25, 437–446.
Deldebbio, J.A., 1991. Sorption of strontium, selenium, cadmium and mercury in soil. Radiochimica Acta 52–3, 181–186.
Dewiere, L., Bugai, D., Grenier, C., Kashparov, V., Ahamdach, N., 2004. Sr-90 migration to the geo-sphere from a waste burial in the Chernobyl exclusion zone. Journal of Environmental Radioactivity 74, 139–150.
Dyer, A., Chow, J.K.K., Umar, I.M., 2000. The uptake of caesium and strontium radioisotopes onto clays. Journal of Materials Chemistry 10, 2734–2740.
Edwards, L., Kusel, K., Drake, H., Kostka, J.E., 2007. Electron flow in acidic subsurface sediments co-contaminated with nitrate and uranium. Geochimica et Cosmochimica Acta 71, 643–654.
Fernandez, J.M., Piault, E., Macouillard, D., Juncos, C., 2006. Forty years of Sr-90 in situ migration: importance of soil characterization in modeling transport phenomena. Journal of Environmental Radioactivity 87, 209–226.
Ferris, F.G., Hallberg, R.O., Lyvén, B., Pedersen, K., 2000. Retention of strontium, cesium, lead and uranium by bacterial iron oxides from a subterranean environment. Applied Geochemistry 15, 1035–1042.
Finch, A.A., Allison, N., Sutton, S.R., Newville, M., 2003. Strontium in coral aragonite: 1. Characterization of Sr coordination by extended absorption X-ray fine structure. Geochimica et Cosmochimica Acta 67, 1189–1194.
Finneran, K.T., Housewright, M.E., Lovley, D.R., 2002. Multiple influences of nitrate on uranium solubility during bioremediation of uranium-contaminated subsurface sediments. Environmental Microbiology 4, 510–516.
Fredrickson, J.K., Zachara, J.M., Balkwill, D.L., Kennedy, D., Li, S.M.W., Kostandarithes, H.M., Daley, M.J., Romine, M.F., Brockman, F.J., 2004. Geomicrobiology of high-level nuclear waste-contaminated vadose sediments at the Hanford Site, Washington State. Applied and Environmental Microbiology 70, 4230–4241.
Fujita, Y., Redden, G.D., Ingram, J.C., Cortez, M.M., Ferris, F.G., Smith, R.W., 2004. Strontium incorporation into calcite generated by bacterial ureolysis. Geochimica et Cosmochimica Acta 68, 3261–3270.
Goto, K., Taguchi, S., Fukue, Y., Ohta, K., Watanabe, H., 1977. Spectrophotometric determination of manganese with 1-(2-pyridylazo)-2-naphthol and a nonionic surfactant. Talanta 24, 752–753.
Greegor, R.B., Pingitore, N.E., Lytle, F.W., 1997. Strontianite in coral skeletal aragonite. Science 275, 1452–1454.
Gurman, S.J., Binsted, N., Ross, I., 1984. A rapid, exact curved-wave theory for EXAFS calculations. Journal of Physics C: Solid State Physics 17, 143–151.
Handley-Sidhu, S., Renshaw, J.C., Moriyama, S., Stolpe, B., Mennan, C., Bagheriasl, S., Yong, P., Stamboulis, A., Paterson-Beedle, M., Sasaki, K., Pattrick, R.A.D., Lead, J.R., Macaskie, L.E., 2011. Uptake of Sr^{2+} and Co^{2+} into biogenic hydroxyapatite: implications for biomineral ion exchange synthesis. Environmental Science and Technology 45, 6985–6990.
Harris, S.J., Mortimer, R.J.G., 2002. Determination of nitrate in small water samples (100 mu L) by the cadmium–copper reduction method: a manual technique with application to the interstitial waters of marine sediments. International Journal of Environmental and Analytical Chemistry 82, 369–376.
Hartman, M.J., Morasch, L.F., Webber, W.D., 2007. Summary of Hanford Site Groundwater Monitoring for Fiscal Year 2006. PNNL-16346-SUM, Pacific Northwest National Laboratory. Richland, W.A. March 2007Available on: http://ifchanford.pnnl.gov/pdfs/16346_sum.pdf.
Hofmann, A., van Beinum, W., Meeussen, J.C.L., Kretzschmar, R., 2005. Sorption kinetics of strontium in porous hydrous ferric oxide aggregates II. Comparison of experimental results and model predictions. Journal of Colloid and Interface Science 283, 29–40.
Hull, L.C., Schafer, A.L., 2008. Accelerated transport of Sr-90 following a release of high ionic strength solution in vadose zone sediments. Journal of Contaminant Hydrology 97, 135–157.
Hussain, S.A., Demirci, S., Özbayoglu, G., 1996. Zeta potential measurements on three clays from Turkey and effects of clays on coal flotation. Journal of Colloid and Interface Science 184, 535–541.
Istok, J.D., Senko, J.M., Krumholz, L.R., Watson, D., Bogle, M.A., Peacock, A., Chang, Y.J., White, D.C., 2004. In situ bioreduction of technetium and uranium in a nitrate-contaminated aquifer. Environmental Science and Technology 38, 468–475.
Jackson, R.E., Inch, K.J., 1989. The in-situ adsorption of strontium-90 in a sand aquifer at the chalk river nuclear laboratories Canada. Journal of Contaminant Hydrology 4, 27–50.
Langley, S., Gault, A.G., Ibrahim, A., Takahashi, Y., Renaud, R., Fortin, D., Clark, I.D., Ferris, F.G., 2009a. Sorption of strontium onto bacteriogenic iron oxides. Environmental Science and Technology 43, 1008–1014.
Langley, S., Gault, A.G., Ibrahim, A., Takahashi, Y., Renaud, R., Fortin, D., Clark, I.D., Ferris, F.G., 2009b. Strontium desorption from bacteriogenic iron oxides (BIOS) subjected to microbial Fe(III) reduction. Chemical Geology 262, 217–228.
Law, G.T.W., Geissler, A., Boothman, C., Burke, I.T., Livens, F.R., Lloyd, J.R., Morris, K., 2010. Role of nitrate in conditioning aquifer sediments for technetium bioreduction. Environmental Science and Technology 44, 150–155.
Law, G.T.W., Geissler, A., Lloyd, J.R., Burke, I.T., Livens, F.R., Boothman, C., McBeth, J.M., Morris, K., 2011. Uranium cycling in sediment and biomineral systems. Geomicrobiology Journal 28, 497–506.
Liszewski, M.J., Rosentrater, J.J., Miller, K.E., Batholomay, R.C., 1998. Strontium distribution coefficients of surficial and sedimentary interbed samples from the Idaho National Engineering and Environmental Laboratory, Idaho. US Geological Survey — Water Resources Investigations Report 98-4073. .
Lloyd, J.R., 2003. Microbial reduction of metals and radionuclides. FEMS Microbiology Reviews 27, 411–425.
Lloyd, J.R., Renshaw, J.C., 2005. Bioremediation of radioactive waste: radionuclide-microbe interactions in laboratory and field-scale studies. Current Opinion in Biotechnology 16, 254–260.
Lovley, D.R., Phillips, E.J.P., 1986. Availability of ferric iron for microbial reduction in bottom sediments of the fresh-water tidal Potomac River. Applied and Environmental Microbiology 52, 751–757.
Mason, C.F.V., Lu, N., Conca, J., 2000. Radioactive strontium- and caesium-contaminated sites: characterisation, transport, and remedial options. Nuclear Physical Methods in Radioecological Investigations of Nuclear Test Sites, 31, pp. 89–97.
McBeth, J.M., Lear, G., Lloyd, J.R., Livens, F.R., Morris, K., Burke, I.T., 2007. Technetium reduction and reoxidation in aquifer sediments. Geomicrobiology Journal 24, 189–197.
McKenzie, H., Armstrong-Pope, N., 2010. Groundwater Annual Report 2010. Sellafield Ltd. Technical Report TECH000613Available on: http://www.sellafieldsites.com/land/documents/Groundwater_Annual_Report_2010.pdf.
McKinley, J.P., Zachara, J.M., Smith, S.C., Liu, C., 2007. Cation exchange reactions controlling desorption of Sr-90 from coarse-grained contaminated sediments at the Hanford site, Washington. Geochimica et Cosmochimica Acta 71, 305–325.
Mitchell, A.C., Ferris, F.G., 2005. The coprecipitation of Sr into calcite precipitates induced by bacterial ureolysis in artificial groundwater: temperature and kinetic dependence. Geochimica et Cosmochimica Acta 69, 4199–4210.
Nikitenko, S., Beale, A.M., Van der Eerden, A.M.J., Jacques, S.D.M., Leynaud, O., O'Brien, M.G., Detollenaere, D., Kaptein, R., Weckhysen, B.M., 2008. Implementation of a combined SAXS/WAXS/QEXAFS set-up for time-resolved in situ experiments. Journal of Synchrotron Radiation 15, 632–640.
O'Day, P.A., Newville, M., Neuhoff, P.S., Sahai, N., Carroll, S.A., 2000. X-ray absorption spectroscopy of strontium(II) coordination — I. Static and thermal disorder in crystalline, hydrated, and precipitated solids and in aqueous solution. Journal of Colloid and Interface Science 222, 184–197.
Parkman, R.H., Charnock, J.M., Livens, F.R., Vaughan, D.J., 1998. A study of the interaction of strontium ions in aqueous solution with the surfaces of calcite and kaolinite. Geochimica et Cosmochimica Acta 62, 1481–1492.
Parmar, N., Warren, L.A., Roden, E.E., Ferris, F.G., 2000. Solid phase capture of strontium by the iron reducing bacteria *Shewanella alga* strain BrY. Chemical Geology 169, 281–288.
Pingitore, N.E., Lytle, F.W., Davies, B.M., Eastman, M.P., Eller, P.G., Larson, E.M., 1992. Mode of incorporation of Sr^{2+} in calcite — determination by X-ray absorption-spectroscopy. Geochimica et Cosmochimica Acta 56, 1531–1538.
Priest, N.D., Kuyanova, Y., Pohl, P., Burkitbayev, M., Mitchell, P.I., Vintro, L.L., Strilchuk, Y.G., Lukashenko, S.N., 2008. Strontium-90 contamination within the Semipalatinsk nuclear test site: results of SEMIRAD1 and SEMIRAD2 projects — contamination levels and projected doses to local populations. Nuclear Risks in Central Asia, pp. 87–105.
Ravel, B., Newville, M., 2005. Athena, Artemis, Hephaestus: data analysis for X-ray absorption spectroscopy using IFEFFIT. Journal of Synchrotron Radiation 12, 537–541.
Riley, R.G., Zachara, J.M., 1992. Chemical Contaminants on DOE Lands and Selection of Contaminant Mixtures for Subsurface Science Research, DOE/ER-0547T. US Department of Energy, p. 77.
Roden, E.E., Leonardo, M.R., Ferris, F.G., 2002. Immobilization of strontium during iron biomineralization coupled to dissimilatory hydrous ferric oxide reduction. Geochimica et Cosmochimica Acta 66, 2823–2839.
Sahai, N., Carroll, S.A., Roberts, S., O'Day, P.A., 2000. X-ray absorption spectroscopy of strontium(II) coordination — II. Sorption and precipitation at kaolinite, amorphous silica, and goethite surfaces. Journal of Colloid and Interface Science 222, 198–212.
Senko, J.M., Mohamed, Y., Dewers, T.A., Krumholz, L.R., 2005. Role for Fe(III) minerals in nitrate-dependent microbial U(VI) oxidation. Environmental Science and Technology 39, 2529–2536.
Small, T.D., Warren, L.A., Roden, E.E., Ferris, F.G., 1999. Sorption of strontium by bacteria, Fe(III) oxide, and bacteria-Fe(III) oxide composites. Environmental Science and Technology 33, 4465–4470.
Solecki, J., 2005. Investigation of Sr-85 adsorption on selected soils of different horizons. Journal of Environmental Radioactivity 82, 303–320.

Stephens, J.A., Whicker, F.W., Ibrahim, S.A., 1998. Sorption of Cs and Sr to profundal sediments of a Savannah River Site reservoir. Journal of Environmental Radioactivity 38, 293–315.

Stookey, L.L., 1970. Ferrozine— a new spectrophotometric reagent for iron. Analytical Chemistry 42, 779–781.

Tenderholt, A., Hedman, B., Hodgson, K.O., 2007. PySpline: a modern, cross-platform program for the processing of raw averaged XAS edge and EXAFS data. In X-Ray Absorption Fine Structure-XAFS13, pp. 105–107.

Tesoriero, A.J., Pankow, J.F., 1996. Solid solution partitioning of Sr^{2+}, Ba^{2+}, and Cd^{2+} to calcite. Geochimica et Cosmochimica Acta 60 1063-1063.

Thorpe, C.L., Law, G.T.W., Boothman, C., Lloyd, J.R., Burke, I.T., Morris, K., 2012. The synergistic effect of high nitrate concentrations on sediment bioreduction. Geomicrobiology Journal 29, 484–493.

Tomic, S., Searle, B.G., Wander, A., Harrison, N.M., Dent, A.J., Mosselmans, J.F., Inglesfield, J.E., 2005. New tools for the analysis of EXAFS: the DL_EXCURV package. CCLRC Technical Report DL-TR-2005-00. . ISSN 1362-0207, Daresbury SRS 2005.

Viollier, E., Inglett, P.W., Hunter, K., Roychoudhury, A.N., Van Cappellen, P., 2000. The ferrozine method revisited: Fe(II)/Fe(III) determination in natural waters. Applied Geochemistry 15, 785–790.

Warren, L.A., Maurice, P.A., Parmar, N., Ferris, F.G., 2001. Microbially mediated calcium carbonate precipitation: implications for interpreting calcite precipitation and for solid-phase capture of inorganic contaminants. Geomicrobiology Journal 18, 93–115.

Wilkins, M.J., Livens, F.R., Vaughan, D.J., Beadle, I., Lloyd, J.R., 2007. The influence of microbial redox cycling on radionuclide mobility in the subsurface at a low-level radioactive waste storage site. Geobiology 5, 293–301.

Wilson, P.D., 1996. Nuclear Fuel Cycle: From Ore to Wastes. Oxford University Press.

Zachara, J.M., Cowan, C.E., Resch, C.T., 1991. Sorption of divalent metals on calcite. Geochimica et Cosmochimica Acta 55, 1549–1562.

Zhuang, J., Yu, G.R., 2002. Effects of surface coatings on electrochemical properties and contaminant sorption of clay minerals. Chemosphere 49, 619–628.